

Spin-Electric Coupling in Lead Halide Perovskites

Artem G. Volosniev,¹ Abhishek Shiva Kumar,¹ Dusan Lorenc,¹ Younes Ashourishokri,¹
Ayan A. Zhumekenov,² Osman M. Bakr,² Mikhail Lemeshko,¹ and Zhanybek Alpichshev^{1,*}

¹*Institute of Science and Technology Austria, Am Campus 1, 3400 Klosterneuburg, Austria*

²*KAUST Catalysis Center (KCC), Division of Physical Sciences and Engineering,*

King Abdullah University of Science and Technology (KAUST), Thuwal 23955-6900, Kingdom of Saudi Arabia

Lead halide perovskites enjoy a number of remarkable optoelectronic properties. To explain their origin, it is necessary to question how the electromagnetic field interacts with these systems. We address it here by studying two classical quantities: Faraday rotation and the complex refractive index in a paradigmatic perovskite $\text{CH}_3\text{NH}_3\text{PbBr}_3$ in a broad wavelength range. We find that the minimal coupling of electromagnetic fields to the $\mathbf{k}\cdot\mathbf{p}$ Hamiltonian is insufficient to describe the observed data even on the qualitative level. To amend this, we demonstrate that there exists a relevant atomic-level coupling between electromagnetic fields and the spin degree of freedom. This spin-electric coupling allows for quantitative description of a number of previous as well as present experimental data. In particular, we use it to show that the Faraday effect in lead halide perovskites is dominated by the Zeeman splitting of the energy levels, and has a substantial beyond-Becquerel contribution. Finally, we present general symmetry-based phenomenological arguments that in the low-energy limit our effective model includes all possible couplings to the electromagnetic field in the linear order.

Originally, lead-halide perovskites (LHP) attracted attention as promising candidates for photovoltaic applications [1–3]. However, it was soon realized that LHP also feature a host of other exceptional but seemingly unrelated optical properties such as efficient THz generation, high harmonic generation and even high-temperature Dicke superluminescence to name a few (see e.g. [4–6] and references therein). This richness of physics arguably makes lead-halide perovskites unique and calls for a better understanding of what makes them so special at the microscopic level. In particular, in view of the growing consensus on the importance of Rashba-type physics in the context of these materials [7–11], there is an urge to have a unified framework for describing the interaction between electromagnetic fields and electronic degrees of freedom in lead halide perovskites.

The band structure of conduction- and valence-band electrons near the chemical potential in LHP is well understood by now. Their quantitative description can be achieved within the $\mathbf{k}\cdot\mathbf{p}$ approach based on spin-orbit-split Pb-based s- and p-orbitals hybridized with neighbouring halide s- and p-orbitals [9]. To include the electromagnetic field in this description, one would naively perform the standard substitution ($\mathbf{k}\rightarrow\mathbf{k}-e\mathbf{A}$). However, as we show below, this leads to a qualitative disagreement with experimental measurements of some classical quantities such as the linear refractive index and Faraday rotation. In this Letter, we show that, in order to achieve a quantitative agreement with experiment, it is necessary to introduce additional coupling terms into the effective model of LHP. Physically these terms are related to the atomic polarization of Pb atoms, and to the details of the electronic structure of LHP, which leads to a very specific Zeeman-type interaction. By using very general arguments, we construct a phenomenological Hamilto-

nian that includes both electric and magnetic fields, and fix the magnitude of each term by comparing the predictions of the theory with our measurements.

We focus on basic optical properties such as frequency-dependent absorption and the dielectric constant $\epsilon(\omega)$, which can provide important insight into the microscopic structure of a material [12, 13]. We also measure the Faraday effect – a rotation of polarization of light that propagates inside a sample in the presence of a magnetic field [14]. One important aspect of this phenomenon is that in order to account for it, one needs to consider the effect of both electric and magnetic fields on the material. This makes it particularly useful for understanding details of the electronic coupling to electromagnetic fields.

Faraday rotation.— The observable that quantifies strength of the Faraday effect in a given medium is the so-called Verdet constant, V , which is defined via $\Theta_F = VBL$, where Θ_F is the angle between the initial and final polarizations; B is the strength of the magnetic field; L is the thickness of the sample. In general, V is a function of frequency of the probing light. As is well known [14], $V(\omega)$ tends to diverge near absorption regions. In many cases this behaviour can be captured by the classical Becquerel formula: $V(\omega) = \gamma \frac{e}{2mc} \omega \frac{\partial n}{\partial \omega}$, with $n(\omega)$ being the (phase) refractive index and $\gamma \approx 1$ is a numeric fitting parameter.

Large Verdet constants have recently been demonstrated in the vicinity of the band gap transition in methylammonium lead bromide perovskites $\text{CH}_3\text{NH}_3\text{PbBr}_3$ [15], suggesting industrial applications of LHP as Faraday rotators. Despite this progress the band edge transition does not allow for a complete understanding of $V(\omega)$. One reason is the extreme sensitivity of $V(\omega)$ on the value of the gap energy Δ , as the Bec-

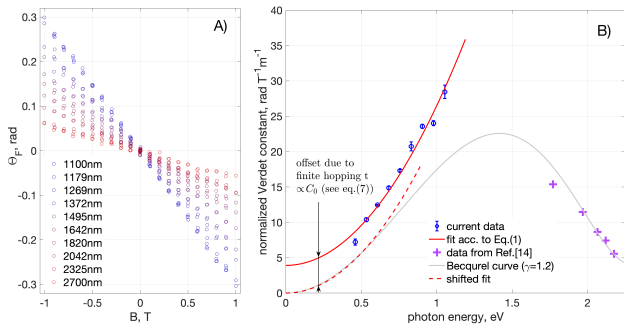


FIG. 1. A) Faraday rotation Θ_F as a function of the magnetic field, B ; B) Normalized Verdet constant $\tilde{V}(\omega)$ extracted from the data in A) as a function of the incident photon energy (blue circles); red curve: fit according to Eq. (1) (see text); purple crosses: high-frequency data extracted from Ref. [15], shown here for comparison; gray curve: normalized Verdet constant $\tilde{V}(\omega)$ computed from the Becquerel formula $\gamma(e/2mc)\omega \partial n/\partial\omega$ with $n(\omega)$ extracted from the data in Fig. 3B. Note that the fit according to Eq. (1) differs from the Becquerel curve only by a constant shift (red dashed curve) at low frequencies.

querel formula suggests; another reason is the presence of a strong exciton near the absorption edge (see Fig. 3B) which dominates $n(\omega)$ in this frequency range, obscuring the details of the underlying basic single-particle physics.

In this Letter, we study the Faraday effect in a bulk single-crystal $\text{CH}_3\text{NH}_3\text{PbBr}_3$ sample in a broad infrared range $\lambda=1100-2700\text{nm}$. The tunable-wavelength probe beam is generated by an optical parametric amplifier. Throughout the experiment the sample was kept in vacuum at $T=260\text{K}$ nominal temperature (cubic phase) in an optical magnet cryostat; the field was varied between $B=\pm 1\text{T}$; the polarization rotation was detected with a pair of balanced pyroelectric IR detectors (see Fig. 1A). High quality bulk single crystal samples of $\text{CH}_3\text{NH}_3\text{PbBr}_3$ were grown by inverse temperature crystallization method as described elsewhere [16, 17]. More experimental details can be found in Supplementary Material.

The measured Faraday rotations as a function of B is presented in Fig. 1A. The slope of each line is proportional to the Verdet coefficient at this wavelength. It is known from general considerations that $V(\omega)$ must be an even function of frequency [18], thus, suggesting the following functional form to analyze the data at low frequencies:

$$V(\omega) = \frac{a_0 + a_2\omega^2}{(\Delta^2 - \omega^2)^2}, \quad (1)$$

where a_0 and a_2 are fitting parameters, and Δ is the band gap. The form of the denominator is motivated by the Becquerel formula [15]. In order to focus on the non-trivial numerator of Eq. (1), we plot in Fig. 1B the “nor-

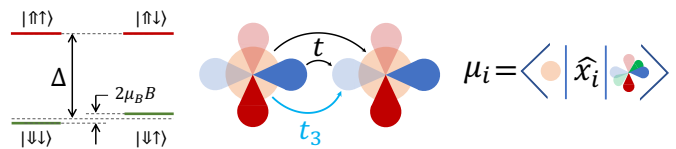


FIG. 2. Basic elements of the effective Hamiltonian. Left: Conduction band made of spin-orbit coupled p-type orbitals ($J=1/2$); and valence band made of s-type orbitals ($J=1/2$). Zeeman interaction projected on this basis acts only on the valence band. Middle: inter-site hopping between s- and p-orbitals; t and t_3 correspond to the inter- and intra-orbital hoppings respectively. Right: On-site electric field-induced hybridization between s- and p-orbitals. See Eq. (2) for the definition of the basis states.

malized” Verdet constant $\tilde{V}(\omega) = V(\omega) \cdot (1 - (\omega/\Delta)^2)^2$. As can be seen in Fig. 1B the simple curve $a_0 + a_2\omega^2$ is indeed providing a good fit. As will be shown below, the fact that the value of a_0 is finite indicates the importance of electron hopping at low frequencies.

Theoretical considerations.— Our starting point for describing the observed frequency dependence of $V(\omega)$ is the effective low-energy Hamiltonian introduced phenomenologically in [19] and in [9] via the $\mathbf{k}\cdot\mathbf{p}$ method [20]. This approach is based upon the fact that the low-energy optoelectronic properties of APbX_3 ($A=\text{Cs}, \text{CH}_3\text{NH}_3$; $X=\text{Cl}, \text{Br}, \text{I}$) can be qualitatively understood from transitions between four basis states originating from $J=1/2$ spin-orbit coupling of p- and s-like states mostly associated with Pb atoms [21]. We introduce the following notation to refer to these states:

$$\begin{aligned} |\uparrow\uparrow\rangle &= -(|p_z\rangle|\uparrow\rangle + (|p_x\rangle + i|p_y\rangle)|\downarrow\rangle)/\sqrt{3}, \\ |\uparrow\downarrow\rangle &= (|p_z\rangle|\downarrow\rangle - (|p_x\rangle - i|p_y\rangle)|\downarrow\rangle)/\sqrt{3}, \\ |\downarrow\uparrow\rangle &= |s\rangle|\uparrow\rangle, \quad |\downarrow\downarrow\rangle = |s\rangle|\downarrow\rangle. \end{aligned} \quad (2)$$

Here the thick and thin arrows correspond to the orbital (valence/conduction) and total angular momentum (quasi-spin) $J=1/2$ states respectively. In the vicinity of the high-symmetry R -point (shifted such that $\mathbf{k}\equiv 0$), the effective Hamiltonian can be written as ($\hbar=1$):

$$H_{\mathbf{k}} = \frac{1}{2} (\Delta + t_3(\mathbf{k}a)^2) \tau_3 \otimes \sigma_0 + 2at \tau_2 \otimes \sigma_\alpha k^\alpha. \quad (3)$$

Here, t_3 and t are the intra- and inter-orbital hopping integrals respectively (Fig. 2 middle); a is the lattice constant; τ_α and σ_α are the Pauli matrices acting on the orbital and quasi-spin respectively (compare with [19]). In order to account for the Faraday effect, one needs to couple electromagnetic field to this Hamiltonian. The most obvious way to do so is to employ minimal coupling and a Zeeman term in Eq. (3). However, as it turns out, in this case the normalized Verdet constant $\tilde{V}(\omega)$ is independent of frequency contrary to experiment (see below).

In view of this qualitative disagreement, it is necessary to look more carefully at the interaction of electrons

with electromagnetic fields. One factor naturally missing in minimal coupling to the $\mathbf{k}\cdot\mathbf{p}$ Hamiltonian is on-site “atomic” polarization due to the applied electric field. Direct calculation of the matrix elements of $q\mathbf{E}\cdot\mathbf{r}$ over the basis in Eq. (2) produces an extra “spin-electric” term in the Hamiltonian (see Fig. 2):

$$H_E = \mu^{\alpha\beta}\tau_1 \otimes \sigma_\alpha E_\beta = \mu\tau_1 \otimes \vec{\sigma}\cdot\vec{E}. \quad (4)$$

Here, $q = -|e|$ is the charge of electron; $\mu^{\alpha\beta} = q\langle s|r^\alpha|p_\beta\rangle = \mu\delta^{\alpha\beta}$ is the atomic dipole moment. We expect that $\mu \sim qa_0$, a_0 being the radius of Pb atom.

Next, we consider magnetic coupling. Note that the ($J = 1/2$)-quasi-spin is not identical to the actual spin, and the Zeeman term projected on the basis in Eq. (2) will be:

$$H_B = \mu_B \left(\frac{\tau_3 - \tau_0}{2} \right) \otimes \vec{\sigma}\cdot\vec{B}. \quad (5)$$

As this form suggests, only the valence band experiences Zeeman splitting (see Fig. 2). With these considerations, our effective Hamiltonian $H = H_k + H_E + H_B$ reads as

$$H = \frac{1}{2} (\Delta + \epsilon(\mathbf{k})) \tau_3 \otimes \sigma_0 + 2at \tau_2 \otimes \sigma_\alpha Q^\alpha(\mathbf{k}) + \mu\tau_1 \otimes \vec{\sigma}\cdot\vec{E} + (\mu_B/2)(\tau_3 - \tau_0) \otimes \vec{\sigma}\cdot\vec{B}, \quad (6)$$

where $\epsilon(\mathbf{k})$ and $Q^\alpha(\mathbf{k})$ are the extensions of the corresponding functions in Eq. (3) across the Brillouin zone. These functions reflect the band structure; apart from general symmetry properties (see the discussion below) their exact forms are not known, however, these are not relevant for the low-energy effective theory and can be used as fitting factors. One possible form is $\epsilon(\mathbf{k}) = \sum_{\alpha=1}^3 2at_3 (1 - \cos(k_\alpha a))$; $Q_\alpha(\mathbf{k}) = \sin(k_\alpha a)$.

The Hamiltonian in Eq. (6) allows us to calculate the low-frequency Verdet coefficient. Assuming that $t_3 \ll \Delta$, we derive the expression that agrees with Eq. (1):

$$V = -\frac{\mu_B}{2c\epsilon_0 n a^3} \frac{4\Delta\mu^2\omega^2 + C_0}{(\Delta^2 - \omega^2)^2}, \quad (7)$$

where n is the refractive index, C_0 is a constant that depends on t and the specific form of $Q_\alpha(\mathbf{k})$ (see the joint publication for a detailed derivation). First of all, we note that in the limit $\mu=0$ (pure minimal coupling to Eq. (3)) $V(\omega) \sim 1/(\Delta^2 - \omega^2)^2$, which qualitatively disagrees with experimental data (Fig. 1B). In the opposite limit $t=0$, $C_0 = 0$, and hence $V(\omega=0) = 0$. Therefore the actual $V(\omega)$ can be accounted for only if both μ and t are finite. It is also noteworthy that around $\omega = 0$, the Bequerel curve computed for the data in Fig. 3B and γ chosen to match the high frequency data [15], differs from the fit according to Eq. (1) by only a constant offset (Fig. 1B), in agreement with Eq. (7).

Determination of μ and μ_B .— The spin-electric term is essential to capture the observed quadratic frequency

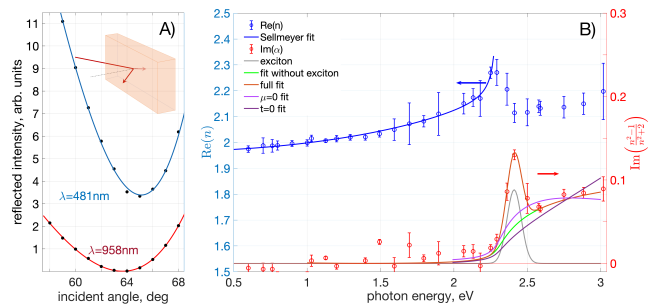


FIG. 3. A) Reflectivity (p-polarization) as a function of the incident angle for two different wavelengths with Fresnel fits to extract the complex refractive index. Note that reflectivity has a finite minimum for $\hbar\omega > \Delta$ reflecting a non-zero imaginary part of $n(\omega)$. Inset: Brewster angle measurement. B) Blue: Experimental $\text{Re}(n)$ (dots) with a Sellmeyer fit (solid curve); Red dots: Imaginary part of polarizability extracted from the imaginary part of the refractive index; Green curve: fit with $t = 0.6\text{eV}$ (t is fixed here to the expected value [9]) and $\mu = -0.29qa$, see Eq. (8); Magenta curve: fit with $t = 1.08\text{eV}$ and $\mu = 0$, see Eq. (8); Purple curve: fit with $t = 0$ and $\mu = -0.64qa$, see Eq. (8); Gray: exciton peak Gaussian fit; Red curve: full fit (sum of green and gray curves). Note that both t and μ terms are necessary for a faithful fit.

dependence of the normalized Verdet constant $\tilde{V}(\omega)$, see Eq. (1). To estimate the value on μ we need additional data since μ enters the corresponding part of Eq. (7) as a product with the unknown magnetic moment μ_B . Therefore, we measure the complex refractive index. This quantity has been previously measured on micro-scale crystals $\text{CH}_3\text{NH}_3\text{PbBr}_3$ [22]. In order to avoid possible effects of the difference in sample geometry, we perform a complementary measurement of the refractive index $n(\omega)$ in a bulk single crystal $\text{CH}_3\text{NH}_3\text{PbBr}_3$ by measuring the reflection of the beam as a function of the incident angle near the Brewster minimum. By fitting the angle dependence using the Fresnel expressions [14], one can extract n . This is similar to the previous experiment [23], however we also go into shorter wavelengths ($\hbar\omega > \Delta$). In this regime the refractive index becomes complex, $n(\omega) = n + ik$. The imaginary part k manifests itself as a finite minimal reflectivity (see Fig. 3; and Supplementary Material)

Complex-valued n can be connected to the polarizability $\alpha(\omega)$ via the Lorentz-Lorenz relation (see, e.g., [24, 25]). For the purpose of determining the low-energy parameters, we are most interested in the imaginary part of $\alpha(\omega)$ since, unlike the real part, it is “local” in frequency and does not receive contributions from the inaccessible high-energy degrees of freedom. The calculation based on Eq. (6) yields for the imaginary part of polarizability (see the joint publication for a detailed derivation):

$$\text{Im}\{\alpha(\omega)\} \simeq \frac{1}{(2\pi)^3} \int_{BZ} \frac{\left(\mu - 2t \frac{q}{\omega} \frac{\partial Q_3}{\partial k_3} \right)^2 d\mathbf{k}}{\Delta + \epsilon(\mathbf{k}) - \omega - i\Gamma/2}. \quad (8)$$

To extract the value of μ by fitting Eq. (8) to the experimental data, we first need to estimate the other parameters that enter Eq. (8): $\Delta \approx 2.3\text{eV}$ is known from optical measurements (see, e.g., Refs. [16, 26–28], and Fig. 3); $t \approx 0.6\text{eV}$ and the bandwidth $t_3 \approx 0.9\text{eV}$ of $\epsilon(\mathbf{k})$ can be estimated by comparing the low-energy electron dispersion (see Eq. (11)) to the first-principles numerical calculations of Ref. [9] where $a = 0.586\text{nm}$ [29]. With these values, fitting of the polarizability gives $\mu \simeq -0.29qa$ (Fig. 3) in line with the natural estimate above; and $\mu_B \simeq -0.4\mu_B$ (Bohr magnetons). The particular form of $\epsilon(\mathbf{k})$ and $Q_\alpha(\mathbf{k})$ as well as the value of Γ does not affect the value of μ noticeably (see the joint publication). Note that Eq. (8) with $\mu = 0$ does not capture the behavior of $\text{Im}\{\alpha\}$, showing importance of the spin-electric coupling term in any analysis of the refractive index.

Discussion.— Now that we have established that the spin-electric coupling is essential to describe response of the material to electromagnetic fields, we argue that the Hamiltonian in Eq (6) is the only possible effective description of the system within our set of approximations. To this end, we fix basic symmetries of the system. For the considered $\text{CH}_3\text{NH}_3\text{PbBr}_3$, these are the cubic point group O_h which includes inversion \hat{I} , and time-reversal symmetry \hat{T} :

$$\hat{T} = i\tau_3 \otimes \sigma_2 \hat{K}, \quad \hat{I} = -\tau_3 \otimes \sigma_0, \quad (9)$$

where \hat{K} is the complex conjugation operator. This set of symmetries is quite restrictive and it turns out that Eq. (6), with $\epsilon(\mathbf{k})$ and $Q_\alpha(\mathbf{k})$ being even and odd functions of \mathbf{k} respectively, is the most general form of a Hamiltonian acting on the basis Eq (2) up to linear order in \vec{E} and \vec{B} .

Identification of the explicit form of H is the central result of our paper. In this part we would like to discuss its physical implications. In the most simple situation with no external fields the electron dispersion near $k = 0$ can be found by simply taking square of H_k :

$$\mathcal{E}_k^2 = \left(\frac{\Delta}{2} + \frac{\hbar^2 k^2}{2m^*} \right)^2 + (2tk a)^2. \quad (10)$$

The energy levels are doubly degenerate, and can be parametrized by the spin degree of freedom – the direction of (quasi-)spin is determined by the direction of the momentum \mathbf{k} . The degeneracy is broken when external electric field \vec{E} is applied. This can be seen most easily seen by squaring the Hamiltonian with $B = 0$:

$$H^2 = \left(\mathcal{E}_k^2 + \mu^2 |\vec{E}|^2 \right) + \tau_3 \otimes \left[\vec{E} \cdot (\vec{k} \times \vec{\sigma}) \right]. \quad (11)$$

The degeneracy is indeed lifted and the splitting has a clear Rashba-type form (see Fig. 4A). Notice that both the conduction and valence bands are split, in agreement with experiment [11] and *ab initio* theory [30].

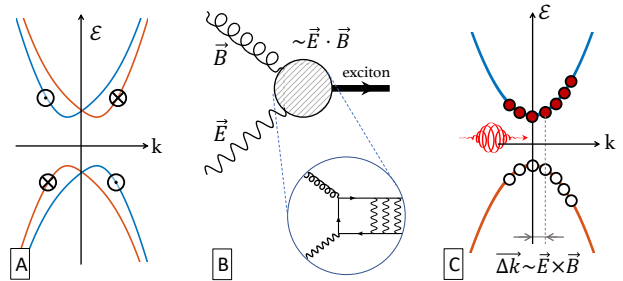


FIG. 4. A) Rashba splitting as follows from the interplay of the hopping and spin-electric terms; B) Axion-type ($\vec{E} \cdot \vec{B}$) term as a result of the spin-electric and the regular Zeeman terms; C) Photo-induced momentum shift under circularly polarized irradiation as a result of the spin-electric and the orbital-selective Zeeman terms.

In the more complex case of finite \vec{E} and \vec{B} , mixing between H_E and H_B can give rise to magneto-electric phenomena taking the following forms:

$$\delta H_{ax} \sim \tau_1 \otimes \sigma_0 (\vec{E} \cdot \vec{B}), \quad \delta H_{pc} \sim \tau_2 \otimes \vec{\sigma} \cdot [\vec{E} \times \vec{B}] \quad (12)$$

Both terms are of the order of $\sim (\mu_B B)(\mu E)/\Delta$. As the structure suggest, δH_{ax} describes what is known in high-energy physics as axion electrodynamics [31]. In the case of perovskites the role of the axionic field ϕ_{ax} is played by a certain exciton (Fig. 4B) [32]. δH_{pc} describes in particular the effect of circularly polarized radiation. Comparing it with H_k one can see that it gives rise to a shift in \mathbf{k} -space in the direction of the incident beam. The possible physical manifestation is a photocurrent along the Poynting vector in a photoexcited perovskite sample (Fig. 4C).

In conclusion, we have analyzed the Faraday effect in $\text{CH}_3\text{NH}_3\text{PbBr}_3$ in a broad wavelength range. We find that in order to describe the observed frequency dependence of the Verdet constant one needs to consider the local atomic response to applied electric field. We find that the coupling has a specific “spin-electric” form. This allows for a quantitative description the data. We argue that at the assumed level of approximation, the proposed Hamiltonian Eq. (6) includes all the terms allowed by the symmetry of the system. Finally, we analyze the implications of introducing the spin-electric term and conclude that in addition to accounting for the widely accepted Rashba splitting, it predicts novel physics such axion electrodynamics in lead-halide perovskites.

We thank Maksym Serbyn, Areg Ghazaryan and Nuh Gedik for useful discussions; M.L. acknowledges support by the European Research Council (ERC) Starting Grant No. 801770 (ANGULON).

- * alpishev@ist.ac.at
- [1] M. Grätzel, The light and shade of perovskite solar cells, *Nature Mater* **13**, 838 (2014).
 - [2] M. Saliba, T. Matsui, J.-Y. Seo, K. Domanski, J.-P. Correa-Baena, M. K. Nazeeruddin, S. M. Zakeeruddin, W. Tress, A. Abate, A. Hagfeldt, and M. Gratzel, Cesium-containing triple cation perovskite solar cells: improved stability, reproducibility and high efficiency, *Energy Environ. Sci.* **9**, 1989 (2016).
 - [3] D. Shi, V. Adinolfi, R. Comin, M. Yuan, E. Alarousu, A. Buin, Y. Chen, S. Hoogland, A. Rothenberger, K. Katsiev, Y. Losovyj, X. Zhang, P. A. Dowben, O. F. Mohammed, E. H. Sargent, and O. M. Bakr, Low trap-state density and long carrier diffusion in organolead trihalide perovskite single crystals, *Science* **347**, 519 (2015).
 - [4] A. Ferrando, J. P. M. Pastor, and I. Suárez, Toward metal halide perovskite nonlinear photonics, *The Journal of Physical Chemistry Letters* **9**, 5612 (2018).
 - [5] Y. Zhou, Y. Huang, X. Xu, Z. Fan, J. B. Khurgin, and Q. Xiong, Nonlinear optical properties of halide perovskites and their applications, *Applied Physics Reviews* **7**, 041313 (2020).
 - [6] G. Findik, M. Biliroglu, D. Seyitliyev, J. Mendes, A. Barrette, H. Ardekani, L. Lei, Q. Dong, F. So, and K. Gundogdu, High-temperature superfluorescence in methyl ammonium lead iodide, *Nature Photonics* **15**, 676 (2021).
 - [7] F. Zheng, L. Z. Tan, S. Liu, and A. M. Rappe, Rashba spin-orbit coupling enhanced carrier lifetime in $\text{CH}_3\text{NH}_3\text{PbI}_3$, *Nano Letters* **15**, 7794 (2015).
 - [8] E. Mosconi, T. Etienne, and F. D. Angelis, Rashba band splitting in organohalide lead perovskites: Bulk and surface effects, *The Journal of Physical Chemistry Letters* **8**, 2247 (2017).
 - [9] M. A. Becker, R. Vaxenburg, G. Nedelcu, P. C. Sercel, A. Shabaev, M. J. Mehl, J. G. Michopoulos, S. G. Lambrakos, N. Bernstein, J. L. Lyons, and et al., Bright triplet excitons in caesium lead halide perovskites, *Nature* **553**, 189–193 (2018).
 - [10] E. Lafalce, E. Amerling, Z.-G. Yu, P. C. Sercel, L. Whittaker-Brooks, and Z. V. Vardeny, Rashba splitting in organic–inorganic lead–halide perovskites revealed through two-photon absorption spectroscopy, *Nature Communications* **13**, 483 (2022).
 - [11] D. Niesner, M. Wilhelm, I. Levchuk, A. Osvet, S. Shrestha, M. Batentschuk, C. Brabec, and T. Fauster, Giant rashba splitting in $\text{CH}_3\text{NH}_3\text{PbBr}_3$ organic-inorganic perovskite, *Physical Review Letters* **117**, 126401 (2016).
 - [12] M. A. Green, Y. Jiang, A. M. Soufiani, and A. Ho-Baillie, Optical properties of photovoltaic organic–inorganic lead halide perovskites, *The Journal of Physical Chemistry Letters* **6**, 4774 (2015).
 - [13] A. M. A. Leguy, P. Azarhoosh, M. I. Alonso, M. Campoy-Quiles, O. J. Weber, J. Yao, D. Bryant, M. T. Weller, J. Nelson, A. Walsh, M. van Schilfgaarde, and P. R. F. Barnes, Experimental and theoretical optical properties of methylammonium lead halide perovskites, *Nanoscale* **8**, 6317 (2016).
 - [14] A. Sommerfeld, *Optics (Lectures on Theoretical Physics, Vol. IV)* (Academic Press Inc. (New York), 1954).
 - [15] R. P. Sabatini, C. Liao, S. Bernardi, W. Mao, M. S. Rahme, A. Widmer-Cooper, U. Bach, S. Huang, A. W. Y. Ho-Baillie, and G. Lakhwani, Solution-processed Faraday rotators using single crystal lead halide perovskites, *Advanced Science* **7**, 1902950 (2020).
 - [16] M. I. Saidaminov, A. L. Abdelhady, B. Murali, E. Alarousu, V. M. Burlakov, W. Peng, I. Dursun, L. Wang, Y. He, G. Maculan, A. Goriely, T. Wu, O. F. Mohammed, and O. M. Bakr, High-quality bulk hybrid perovskite single crystals within minutes by inverse temperature crystallization, *Nature Communications* **6**, 8586 (2015).
 - [17] M. I. Saidaminov, A. L. Abdelhady, G. Maculan, and O. M. Bakr, Retrograde solubility of formamidinium and methylammonium lead halide perovskites enabling rapid single crystal growth, *Chemical Communications* **51**, 17658 (2015).
 - [18] H. S. Bennett and E. A. Stern, Faraday effect in solids, *Phys. Rev.* **137**, A448 (1965).
 - [19] H. Jin, J. Im, and A. J. Freeman, Topological insulator phase in halide perovskite structures, *Physical Review B* **86**, 121102 (2012).
 - [20] E. Kane, Chapter 3 (the $k \cdot p$ method), in *Semiconductors and Semimetals*, Vol. 1, edited by R. Willardson and A. C. Beer (Elsevier, 1966) pp. 75–100.
 - [21] T. Umebayashi, K. Asai, T. Kondo, and A. Nakao, Electronic structures of lead iodide based low-dimensional crystals, *Physical Review B* **67**, 155405 (2003).
 - [22] S. Brittman and E. C. Garnett, Measuring n and k at the microscale in single crystals of $\text{CH}_3\text{NH}_3\text{PbBr}_3$ perovskite, *The Journal of Physical Chemistry C* **120**, 616 (2016).
 - [23] C. He, G. Zha, C. Deng, Y. An, R. Mao, Y. Liu, Y. Lu, and Z. Chen, Refractive index dispersion of organic–inorganic hybrid halide perovskite single crystals, *Crystal Research and Technology* **54**, 1900011 (2019).
 - [24] R. W. Boyd, *Nonlinear Optics*, 3rd ed. (Academic Press, Burlington, 2008).
 - [25] R. Feynman, R. Leighton, and M. Sands, *The Feynman Lectures on Physics (Vol 2, Ch. 32). The New Millennium Edition*.
 - [26] I. P. Pashuk, N. S. Pydzirailo, and M. G. Matsko, Exciton absorption, luminescence and resonant raman scattering of light in perovskite CsPbCl_3 and CsPbBr_3 crystals at low temperature, *Sov. Phys. Sol. State* **23**, 1263 (1981).
 - [27] T. Jesper Jacobsson, J.-P. Correa-Baena, M. Pazoki, M. Saliba, K. Schenk, M. Gratzel, and A. Hagfeldt, Exploration of the compositional space for mixed lead halogen perovskites for high efficiency solar cells, *Energy Environ. Sci.* **9**, 1706 (2016).
 - [28] C. Ng, T. Ripolles, and K. e. a. Hamada, Tunable open circuit voltage by engineering inorganic cesium lead bromide/iodide perovskite solar cells, *Sci Rep* **8**, 2482 (2018).
 - [29] The parameters in this work were calculated for CsPbBr_3 which has a very similar lattice to that of $\text{CH}_3\text{NH}_3\text{PbBr}_3$; t was determined from the Kane energy, E_p : $t^2 = E_p/(24m_0a^2)$, where m_0 is the free-space electron mass. The parameter t_3 was determined by the parameters $\gamma_{e,h}$: $t_3 = -(\gamma_e + \gamma_h)/(a^2m_0)$.
 - [30] M. Kim, J. Im, A. J. Freeman, J. Ihm, and H. Jin, Switchable $s = 1/2$ and $j = 1/2$ rashba bands in ferroelectric halide perovskites, *Proceedings of the National Academy of Sciences* **111**, 6900 (2014).
 - [31] A. Sekine and K. Nomura, Axion electrodynamics in topological materials, *Journal of Applied Physics* **129**,

141101 (2021).

[32] $\phi_{ax} \sim \langle \tau_1^{\alpha\beta} \delta^{ab} c_{\alpha a}^\dagger c_{\beta b} \rangle.$